

# Mapping seismic anisotropy using harmonic decomposition of receiver functions: An application to Northern Apennines, Italy

I. Bianchi,<sup>1</sup> J. Park,<sup>2</sup> N. Piana Agostinetti,<sup>1</sup> and V. Levin<sup>3</sup>

Received 22 October 2009; revised 21 September 2010; accepted 4 October 2010; published 18 December 2010.

[1] Isotropic and anisotropic seismic structures across the Northern Apennines (Italy) subduction zone are imaged using a new method for the analysis of teleseismic receiver functions (RFs). More than 13,000 P-wave coda of teleseismic records from the 2003–2007 Retreating–Trench, Extension, and Accretion Tectonics (RETREAT) experiment are used to provide new insights into a peculiar subduction zone between two continental plates that is considered a focal point of Mediterranean evolution. A new methodology for the analysis of receiver functions is developed, which combines both migration and harmonic decomposition of the receiver function data set. The migration technique follows a classical “Common Conversion Point” scheme and helps to focus on a crucial depth range (20–70 km) where the mantle wedge develops. Harmonic decomposition of a receiver function data set is a novel and less explored approach to the analysis of *P*-to-*S* converted phases. The separation of the back-azimuth harmonics is achieved through a numerical regression of the stacked radial and transverse receiver functions from which we obtain independent constraints on both isotropic and anisotropic seismic structures. The application of our method to the RETREAT data set succeeds both in confirming previous knowledge about seismic structure in the area and in highlighting new structures beneath the Northern Apennines chain, where previous studies failed to clearly retrieve the geometry of the subducted interfaces. We present our results in closely spaced profiles across and along the Northern Apennines chain to highlight the convergence of the Tyrrhenian and the Adriatic microplates which differ in their crustal structure where the Adriatic microplate subducts beneath Tuscany and the Tyrrhenian sea. A signature of the dipping Adriatic Moho is clearly observed beneath the Tyrrhenian Moho in a large portion of the forearc region. In the area where the two Mohos overlap, our new analysis reveals the presence of an anisotropic body above the subducted Moho. There is a strong *Ps* converted phase with anisotropic characteristics from the top of the Adriatic plate to a depth of at least 80 km. Because the *Ps* conversion occurs much deeper than similar *Ps* phases in Cascadia and Japan, dehydration of oceanic crust seems unlikely as a causative factor. Rather, the existence of this body trapped between the two interfaces supports the hypothesis of lower crustal delamination in a postsubduction tectonic setting.

**Citation:** Bianchi, I., J. Park, N. Piana Agostinetti, and V. Levin (2010), Mapping seismic anisotropy using harmonic decomposition of receiver functions: An application to Northern Apennines, Italy, *J. Geophys. Res.*, *115*, B12317, doi:10.1029/2009JB007061.

## 1. Introduction

[2] Plate boundaries where continental lithospheres converge differ from ocean-ocean and ocean-continent convergence zones but often share the structural asymmetry associated

with the subduction of one plate into the upper mantle. Possible plate interactions range from classical subduction kinematics in common with oceanic subduction zones [Peacock and Wang, 1999] to transient lithospheric thickening followed by delamination [Channell and Mareschal, 1989]. The Northern Apennines of Italy is marked by continental convergence and a downgoing slab derived from the Adria microplate [Faccenna *et al.*, 2001]. The lithologic structure at the top of the slab should offer a clue to the nature of Apennines convergence. Probed with seismic waves, the top of the slab could be a gradational feature or be bounded by a single sharp interface or multiple interfaces. Teleseismic receiver functions reconstruct the *Ps* converted

<sup>1</sup>Centro Nazionale Terremoti, Istituto Nazionale di Geofisica e Vulcanologia, Rome, Italy.

<sup>2</sup>Department of Geology and Geophysics, Yale University, New Haven, Connecticut, USA.

<sup>3</sup>Department of Geological Sciences, Rutgers University, Piscataway, New Jersey, USA.

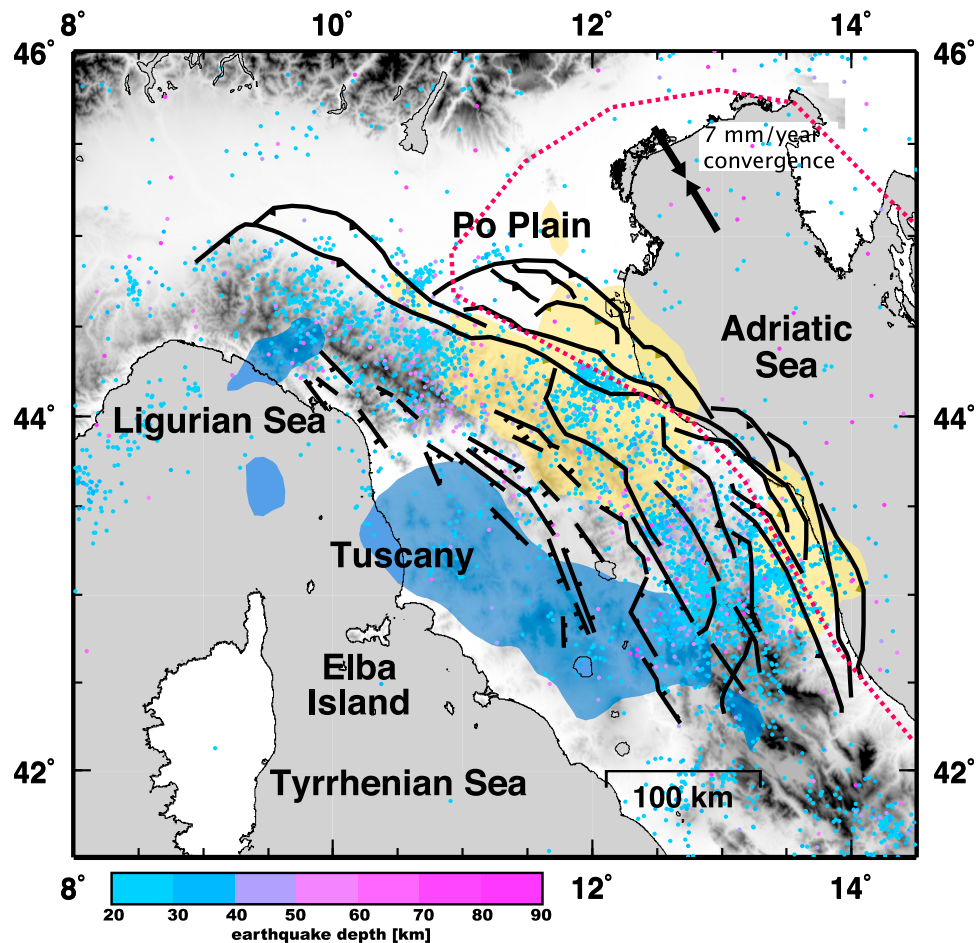


**Figure 1.** Tectonic sketch of the study area. The main tectonic boundaries outline areas that are affected by compression and extension. The arrows indicate the convergence direction between the Eurasia and Africa plates, almost parallel to the strike of the orogen down the Italian peninsula. The Adria microplate boundary is shown by the red-dotted line. Color patches represent the mean  $V_P$  perturbation values in the uppermost 250 km of the mantle beneath Italy from the model of Lucente *et al.* [1999] (Yellow  $-1\%$  and Blue  $+1.5\%$ ). Earthquake foci for events at depth  $> 20$  km are also shown [Chiarabba *et al.*, 2005].

waves from sharp interfaces at depth and can reveal the features consistent with the subduction of oceanic crust, the temporary entrainment of buoyant continental crust, or no downgoing crust at all.

[3] Developed between the European plate and the continental Adriatic microplate, the Northern Apennines (NA) are characterized by an active accretionary wedge that lies below sea level in the northern Adriatic Sea but is subaerial in the Po River Valley. There are active thrust faults at the southern border of the Po River Valley [Picotti and Pazzaglia, 2008; Wilson *et al.*, 2009] and the Apennines orogen is both uplifting and extending (Figure 1). Although most earthquakes are crustal, deeper earthquakes occur along some portions of the NA chain, reaching maximum depths of about 90 km [De Luca *et al.*, 2009; Chiarabba *et al.*, 2005] (Figure 1). Tomographic studies reveal the presence of a westward dipping fast anomaly beneath the NA area, suggesting the sinking of a cold body into the mantle [Lucente *et al.*, 1999]. This body has been associated with the subduction of the Adriatic continental lithosphere as a consequence of the complete consumption of the oceanic lithosphere under the Apennines [Faccenna *et al.*, 2001]. In the foreland, the Adriatic lithosphere has a thickness

of 70–90 km, with the Moho located at about 30–40 km depth [Ponziani *et al.*, 1995]. Earthquakes occur in the upper 20 km of the Adriatic crust and display strike-slip and thrust fault plane solutions, suggesting active compression in the surface [Piccinini *et al.*, 2006]. On the other hand, earthquakes along the Tyrrhenian side of the orogen are no deeper than 10–15 km and mainly show normal fault plane solutions [Piccinini *et al.*, 2009].

[4] Regional tomographic results suggest thinner crust on the Tyrrhenian side than on the Adriatic one, and the velocity contrast between crust and mantle in Tuscany is less strong than beneath the Adriatic Sea [Di Stefano *et al.*, 2009, and references therein]. These results are also supported by thermal data [Pauselli and Federico, 2002] and seismic refraction studies [see Barchi *et al.*, 2006, and references therein]. Therefore in this area two domains (Tyrrhenian and Adriatic) have been identified by Piali *et al.* [1998] and Pauselli *et al.* [2006]. Low-seismic velocity in the uppermost mantle under Tuscany has been suggested from surface wave studies [Keogh *et al.*, 2009; Li *et al.*, 2010]. Measures of SKS splitting in the area highlight a complex link between mantle flow under the NA and orogenic evolution [Salimbeni *et al.*, 2008].

An eastward retreating slab has been invoked as the principal driving force in this area [Malinverno and Ryan, 1986]. A retreating slab determines the present position of the orogen, and has been described as an ongoing and steady state process by, e.g., Faccenna et al. [2004].

[5] Receiver function (RF) analysis is a widely applied technique that uses  $P$ -to- $S$  converted waves, generated at subsurface seismic discontinuities, to map sharp lithologic contrasts at depth. Receiver functions are based on two simple assumptions. First, a plane  $P$ -wave which crosses a planar seismic discontinuity is (partially) converted to an  $S$ -wave. Second, for teleseismic  $P$  waves, source and path effects are recorded on the vertical  $Z$  component of the seismograms. Thus a simple deconvolution of the horizontal components from the vertical gives rise to two time series, a radial (Q-RF) and a transverse (T-RF), which contains the  $P$ -to- $S$  converted waves beneath the receiver [Vinnik, 1977; Langston, 1979; Levin and Park, 1998; Savage, 1998]. The Q-RF contains energy from the isotropic seismic structure beneath the receiver, while T-RF carries information primarily from the anisotropic and/or dipping subsurface structure. Q-RF analysis has been widely used to create images of subduction zones [Ferris et al., 2003; Bannister et al., 2007; Kawakatsu and Watada, 2007; Piana Agostinetti et al., 2009; Nikulin et al., 2009].

[6] Analysis of the transverse receiver functions (T-RF) is far less common. Large T-RF data-sets from single seismic stations have been used to image both anisotropic and dipping structures beneath the receiver [Savage, 1998; Park et al., 2004; Piana Agostinetti et al., 2008b]. Harmonics coefficient analysis, involving both Q and T RF, has been developed for the analysis of subsurface anisotropy [Girardin and Farra, 1998; Bianchi et al., 2008] under isolated seismic stations. However, few imaging techniques, which use data from several seismic stations, join the analysis of the Q and T RF data sets [Tibi et al., 2008; Mercier et al., 2008; Tonegawa et al., 2008].

[7] RF techniques have been already applied to study the NA area. Moho depth in the NA region has been estimated using both temporary [Piana Agostinetti et al., 2002] and permanent [Piana Agostinetti and Amato, 2009] seismic stations. A selection of the RETREAT data set has been employed to estimate crustal properties, i.e., thickness and  $V_P/V_S$ , across the NA chain, using a simple grid search approach [Piana Agostinetti et al., 2008a]. The anisotropic seismic structure of the Adriatic crust has been studied by Levin et al. [2002a], while Roselli et al. [2010] investigated both isotropic and anisotropic structure of the Tyrrhenian crust. Strong evidence of heterogeneity in the crust and upper mantle has been detected under the NA chain, where the previous studies failed to reveal clearly the geometry of the subducted interfaces [Piana Agostinetti et al., 2008a].

[8] In this study, we apply a new technique for RF analysis which allows the separation of the back-azimuth harmonics of the Q and T receiver-function data set as a function of the incoming wavefield direction. Energy due to anisotropic and/or dipping subsurface structures is separated from the isotropic signals and partitioned into back-azimuth harmonics, which become the principal tool for the understanding of subsurface geometries. Data are stacked along profiles which image both isotropic and anisotropic structures. The input data for the profiles are obtained by a common conversion point [Dueker and Sheehan, 1998] stack

technique to focus our analysis between 20 and 70 km depth. In this paper, we first describe the harmonic decomposition and the migration methods. Then, we present results from the analysis of the RETREAT data set, and we discuss our method and the geodynamical implications of the results.

## 2. Data and Method

[9] We use a data set composed of  $\sim 13,000$  RFs obtained from earthquakes at epicentral distances between  $30^\circ$  and  $100^\circ$ , and with  $M > 5.5$ , selected by their high signal-to-noise ratio. Teleseismic events were recorded at 51 broadband, three-component stations, deployed along peninsular Italy, between  $42^\circ\text{N}$  and  $46^\circ\text{N}$  (Figure 2). Forty stations were operated by the RETREAT experiment for durations from 1 to 3 years (10/2003 to 09/2006) [Margheriti et al., 2006]. Ten stations are permanent seismic observatories of the Italian National Seismic network and one station (VLC) belongs to the Mediterranean Network (MedNET). Owing to the long working period of the RETREAT array, we obtained a good back-azimuth coverage (Figure 3). Seismic records are rotated into the LQT reference system to enhance the converted  $P_s$  phases. L is the direction of the hypothetical incoming  $P$  wave (computed using the IASPEI91 model) and Q is perpendicular to L in the vertical-radial plane, i.e., the plane that contains the source and the receiver. T is the ordinary transverse component normal to the L-Q plane. Receiver functions are calculated by a frequency domain algorithm using multitaper correlation estimates [Park and Levin, 2000]. We use a high pass frequency cutoff of 0.5 Hz, which gives us a vertical resolution of approximately 3–5 km.

### 2.1. CCP and Migration

[10] To enhance the continuity of the structures in the study area, we implemented a common conversion point technique [Dueker and Sheehan, 1998; Wilson et al., 2004] (see also auxiliary material).<sup>1</sup> We select five main profiles across the Northern Apennines (Figure 2). Three profiles ( $AA'$ ,  $BB'$ , and  $CC'$ ) share the same direction ( $N18^\circ\text{E}$ ) approximately orthogonal to the strike of the Apennines orogen (in its northern part, between  $9^\circ\text{E}$  and  $13^\circ\text{E}$  longitude). Two profiles ( $DD'$  and  $EE'$ ) are orogen-parallel. For each profile, we divide the area within 40 km of the profile into rectangular boxes 20 km wide, with a 50% overlapping scheme (i.e., each area shares 50% of its surface with the adjacent areas). We select ensembles of RFs (both Q and T) for which surface projections of their conversion points at 40 km depth fall within one of the rectangular areas along the profile. We associate an “ensemble of RFs” with the center of the rectangular area (the “spot,” hereafter). We migrate each individual RF to 40 km depth using the IASPEI91 model (Figure S1). For each spot, we obtain one ensemble of Q-RFs and T-RFs and use them to image the seismic discontinuities in the 20–70-km depth range.

### 2.2. Harmonic Analysis

[11] Both Q and T components contain useful information about the subsurface structure. The isotropic part of the seismic velocity profile at depth mainly affects the Q-RF component, while anisotropy and dipping structures produce

<sup>1</sup>Auxiliary materials are available in the HTML. doi:10.1029/2009JB007061.

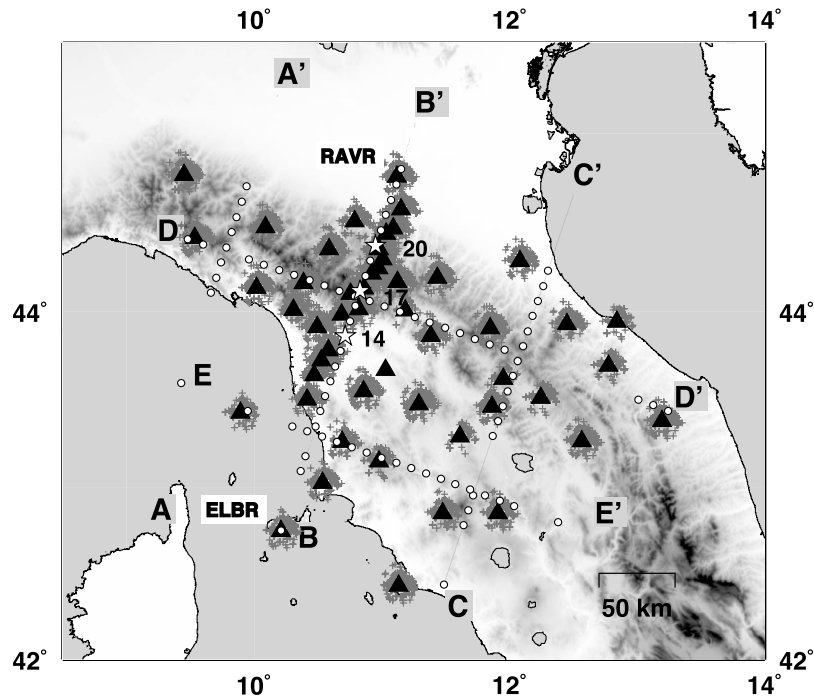


**Figure 2.** Map displaying stations (black triangles) and piercing points at 40-km depth (grey crosses) for the events recorded at the stations used in this study. The map also shows the locations of five virtual profiles of  $P_s$  conversions through our field area. The white dots represent the spots for which we estimated ensemble receiver functions along the virtual profiles. Spots 14, 17, and 20 in profile  $BB'$  are represented by stars. The ELBR (Elba Island) and RAVR (Ravarino) stations at the beginning and the end of  $BB'$  are labeled.

$P$ -to- $S$  conversions recorded on the T-RF component [Levin and Park, 1998; Savage, 1998]. Here, we implemented a technique that allows analyzing both Q and T RFs simultaneously. This is useful in complex tectonic settings, e.g., subduction zones, where both anisotropy and dipping layers are expected, together with strong isotropic seismic velocity jumps.

[12] Our method is based on the extraction of the back-azimuth harmonics of an RF data set as a function of the incoming P-wavefield direction. Here, we assume that at every time step an ensemble of RFs can be expressed as a scaled sum of  $\cos k\phi$  and  $\sin k\phi$ , where  $k$  is the harmonic degree and order, and  $\phi$  is the back azimuth. We limit our analysis to the first three degrees and orders, i.e.,  $k = 0, 1, 2$ . Degree and order  $k = 0$  represents the bulk isotropic variation of the seismic velocities with depth (the “constant” back-azimuth harmonic, hereinafter). For flat interfaces in isotropic media, the T RF contribution vanishes and the signals are expressed only on the  $k = 0$  back-azimuth harmonic of the Q RF data set, obtained with a simple stack of the Q RF components over back-azimuth. The first and second harmonics,  $k = 1, 2$  contain the energy which displays a periodicity of  $2\pi/k$  with the back azimuth  $\phi$  of the incoming P wave. The two-lobed periodicity is expected if a dipping interface or an anisotropic layer with a plunging symmetry axis is present at depth, while a four-lobed periodicity is observed when the subsurface structure includes an anisotropic layer with horizontal symmetry axis [Maupin and Park, 2007]. As shown by Shiomi and Park [2008], amplitudes of Q and T RF back-azimuth harmonics display a  $\pi/2k$  shift for both  $k = 1$  and  $k = 2$ .

[13] Here, we give a brief description of the harmonic decomposition procedure, and we refer the reader to the SOM for details. We expand ensembles of RFs in back-azimuth harmonics for  $k = 1, 2$ . For each value of  $k$  the sum of the Q and

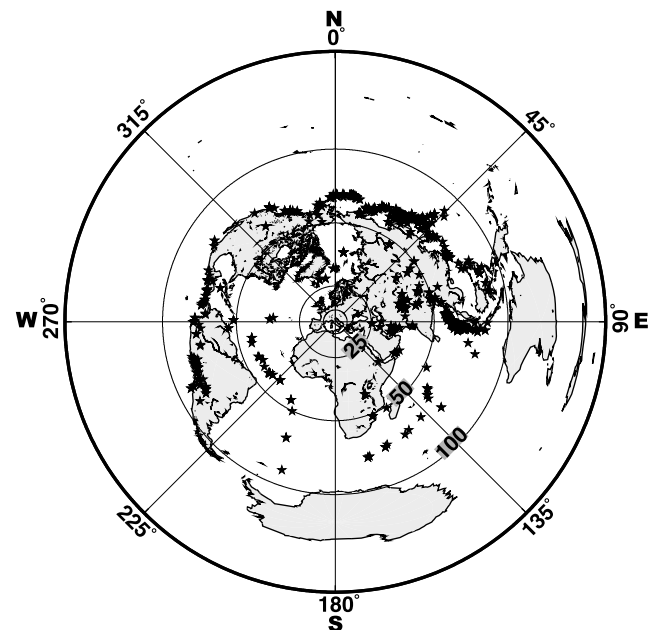


**Figure 3.** Black stars represent the location of teleseismic events recorded at Spot 17 in profile  $BB'$ . Numbers indicate back-azimuth  $\phi$  (rays) and epicentral distance  $\Delta$  (circles).

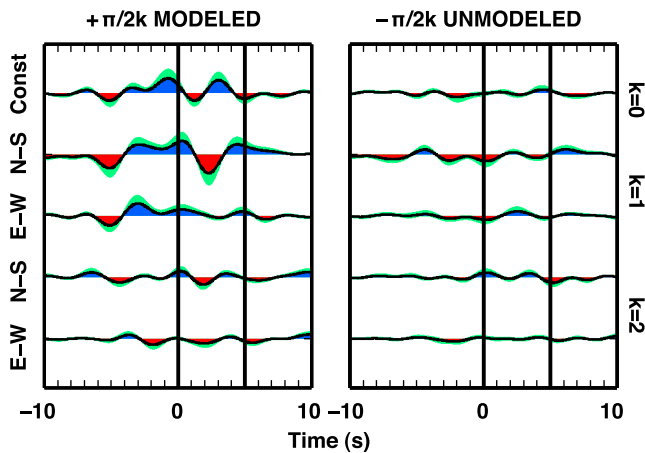


**Figure 4.** Example of the back-azimuth harmonic decomposition for Spot 17 in profile  $BB'$ , showing (left) “Q+iT” component and (right) “Q-iT” component. The constant term is the unweighted stack for all events recorded at the spot. N-S and E-W labels indicate the  $\cos \phi$  and  $\sin \phi$  harmonics terms, respectively. The labels  $k = 0, 1, 2$  indicate the harmonic order.

T RF back-azimuth harmonics with a phase shift of  $+\pi/2k$  (called Q+iT, hereinafter) enhances the effect due to anisotropy or dipping interfaces. A sum of the Q and T RF back-azimuth harmonics with a reverse shift (i.e.,  $-\pi/2k$ , called Q-iT hereinafter) highlights the component of directional variation in our data set that is due to scatterers or complex 3-D heterogeneities. The resulting combined harmonics Q+iT and Q-iT are periodic functions of back azimuth that may be represented as combinations of scaled functions  $\sin k\phi$  and  $\cos k\phi$ , where  $k = 0, 1, 2$  and  $\phi$  is back azimuth. It is useful to examine some simple rules this representation implies. For example, a dipping interface striking E-W will impose a two-lobed pattern on the Q+iT component and no signal on Q-iT component. The maximum Q-RF signal will be expected along the N-S axis, while the maximum T-RF signal will be along the E-W axis. The corresponding representation Q+iT will be proportional to  $\cos \phi$ , while Q-iT will be zero. A similar representation is expected from an anisotropic layer with an axis plunging to either N or S. If the  $\sin \phi$  back-azimuth harmonic dominates instead, maximal amplitudes of the Q-RF and T-RF are E-W and N-S, respectively, and we can expect a dipping plane striking N-S, or an anisotropic symmetry axis plunging either E or W. A significant contribution from either  $\sin 2\phi$  or  $\cos 2\phi$  would indicate near-horizontal orientation of the anisotropic symmetry axis. A significant amplitude on any of the Q-iT components would be worrisome, suggesting deviations from layered structure beneath the receiver. A similar approach was proposed by *Girardin and Farra* [1998] and has been successfully applied to a mantle wedge investigation [*Vinnik et al.*, 2007; *Piana Agostinetti et al.*, 2008a].

[14] Figure 4 shows an example of the decomposition of the  $Q \pm iT$  data-set for the 17th spot along profile  $BB'$  (see Figure 2). RFs are migrated so that 0 time corresponds to the depth of 40 km. Traces marked  $k = 0$  display the component that is constant with back azimuth  $\phi$ . A big negative pulse is present at  $-5$  s, due to the near surface structure, and posi-

tive pulses are present on the Q+iT plot at  $-1$  and  $3$  s time delay, corresponding to interfaces at depth shallower and deeper than 40 km, respectively. The Q-iT part, which should be zero, displays limited energy, likely due to the imperfect back-azimuth coverage of the RF ensemble. To assess the variance of the decomposed  $Q \pm iT$  harmonic traces, we adopt a bootstrap approach, in which the full data set is resampled multiple times ( $> 100$  iterations) to determine the natural variability of parameters estimated from the full data set. The standard deviation of the bootstrapped  $Q \pm iT$  harmonics is indicated by the light green envelopes around the plotted time series.

[15] Other traces in Figure 4 contain higher-order receiver-function harmonics. On the left, the second and third traces show the summation of the Q and T back-azimuth harmonics, with a  $+\pi/2k$  phase shift, for two normal directions (N-S and E-W, respectively). As explained above, this summation enhances  $P$ -to- $S$  conversions which display a  $2\pi/k$  periodicity as a function of back azimuth. Both  $\cos \phi$  and  $\sin \phi$  RF traces show energy in this harmonic, but the  $\cos \phi$  signal seems everywhere stronger than the  $\sin \phi$  signal, suggesting a preferred N-S orientation of the symmetry axis of the underlying structure.

[16] On the right, the second and third traces display the summation of the Q- and T- back-azimuth harmonic with a reverse phase shift, i.e.,  $-\pi/2k$ , displaying signals given by lateral structural variations or scatterers. Energy on the Q-iT plot is limited to the negative times that correspond to very shallow crust, while almost no energy is present at 0–4-s time delays, i.e., at depths corresponding to the uppermost mantle below spot 17. This demonstrates that, while  $Ps$  scattering from subcrustal depths follows the predictions of simple models, scattering by structures in the uppermost crust may be more complicated. The fourth and fifth traces of the left panel show the  $k = 2$  back-azimuth harmonics, which are useful to understand if an anisotropic layer with horizontal axis is present [*Levin and Park*, 1997]. In this study, we find limited energy on the  $k = 2$  back-azimuth harmonics at the frequencies used; therefore we do not consider them further.

### 2.3. Symmetry Directions

[17] Comparing the signals in the  $\cos \phi$  and  $\sin \phi$  back-azimuth harmonics for each spot, we extract information about the symmetry directions of the main features. Plotting the particle motion implied by the  $\cos \phi$  and  $\sin \phi$  back-azimuth harmonics of the RFs for selected time windows gives the trend of apparent symmetry axes at corresponding depths. In Figure 5, we plot the particle motion for the 17th spot along profile  $BB'$ , computed in the 0–5-s time-window. The arrow direction represents the linear trend of the particle motion, estimated by a least squares fit. Arrow length is proportional to maximum elongation in the particle motion plot in Figure 5. Here, we clearly observe a NNE direction, which reflects either a trend of the symmetry axis of anisotropic materials at depth or a dip direction of an inclined seismic discontinuity.

### 2.4. Modeling

[18] To interpret the observed RFs along the different profiles, we produced a set of synthetic RF traces using simple models. We created synthetic records using the RAYSUM

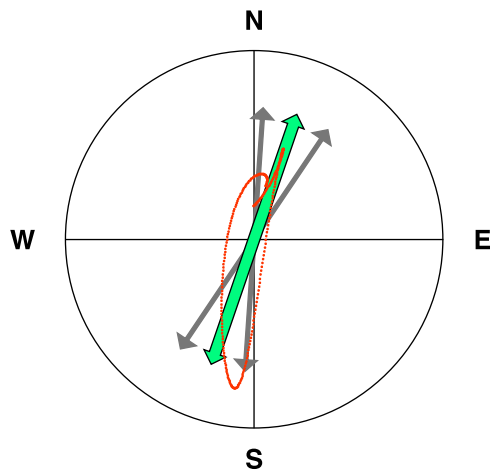


**Figure 5.** Particle motion obtained for the 0–5 s time window relative to the 40-km target migration depth, at spot 17 (black line). The green arrow displays the linear trend of the particle motion. The two grey arrows indicate the  $3\sigma$  error estimate for the first parameter of the linear trend, i.e., the particle motion direction. In this case  $3\sigma$  is roughly  $15^\circ$ .

code [Frederiksen and Bostock, 2000], which models the propagation of a teleseismic wave through a stack of anisotropic layers separated by planar dipping interfaces. For each spot, the procedure previously described for the computation of the observed RF traces is applied to a distribution of teleseismic rays similar to the observed one, to produce the synthetic RF traces. Synthetic and observed RF traces are compared to retrieve the gross seismic structure along a profile. While qualitative information about subsurface geometry is easily deduced from the raw comparison of observed and synthetic RF traces, a more sophisticated inversion scheme would be needed to estimate the elastic properties along the profile.

### 3. Results

#### 3.1. Harmonic Analysis

[19] We apply the procedure for the decomposition described above to each profile (Figure 2), to reconstruct the subsurface features across the study area. For each profile, we plot three sweeps which contain the constant, the  $\cos \phi$  (N–S) and the  $\sin \phi$  (E–W) parts of the decomposition. Positive/negative amplitudes are shown as blue/red pulses in the RF traces. Owing to the overlapping scheme adopted here, the trace at each geographical spot shares data only with its immediate neighbor spots, and the RF traces are migrated in the depth domain (Figures 6–10) using CCP migration (Figure S1). Our strategy focusses the RFs in the 20–70-km depth interval.

[20] Profile  $BB'$  crosses the Apennines along a dense line of seismic stations, so that its spots are estimated from a larger number of RFs than the other profiles. Later, we extend our observation to the other profiles, to find correspondences and variations of the main features across the study area. Profile  $BB'$  (Figure 7) is 270 km long and includes data from ELBR station (Isola d'Elba, Tyrrhenian sea) to RAVR (Ravarino, Po Plain). RF traces at individual spots are estimated from at least 120 distinct event-receiver combinations, i.e., tele-

seismic records. Large amplitudes are present both on the constant and  $\cos \phi$  back-azimuth harmonics, while the  $\sin \phi$  back-azimuth harmonic displays lower amplitude than the other two components. The delay time in the plots is referenced to the migration target at 40-km depth, so that pulses at negative delay time correspond to interfaces shallower than 40 km.

[21] Although significant signal is present in  $-3$  to  $-5$  s range of the three components, we do not attempt to reproduce it, as this likely represents complex near surface structure. Two main features are present in the constant harmonic: a positive phase starts at  $-2$  s in the westernmost part of the profile and ends at  $-1$  sec at  $X = 170$  km, i.e., under the crest of the chain; another well-defined positive phase shows up in the Adriatic side displaying a dipping behavior toward the SW direction, i.e., its arrival time changes from 0 s in the easternmost side ( $X = 240$  km) to 6 s at about  $X = 130$  km. On the  $\cos \phi$  plot, we observe that strong energy, displayed as a double negative/positive pulse, is present where the two pulses described above overlap. The delay time of this double pulse grows toward the SW along a segment about 60 km long, and since energy is present only on the  $\cos \phi$  component,

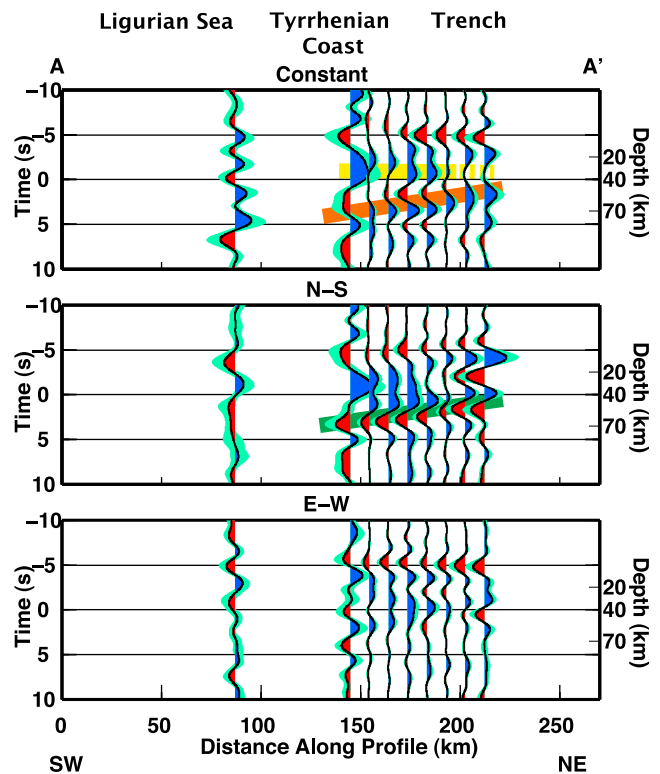


**Figure 6.** RF data set along profile  $AA'$ , displayed as constant,  $\cos \phi$  (N–S) and  $\sin \phi$  (E–W) back-azimuth harmonics. Blue and red pulses indicate positive and negative amplitudes, respectively. Colored stripes highlight the main features: yellow for the Tyrrhenian Moho, orange for the Adriatic Moho, and green for the 3-D feature. The X-axis is distance along the profile in km, the Y-axis is  $P_s$  delay time (scalable to depth), in s (km). The delay time in the plots is referenced to the migration target at 40 km depth, so that pulses at negative delay time correspond to interfaces shallower than 40 km.

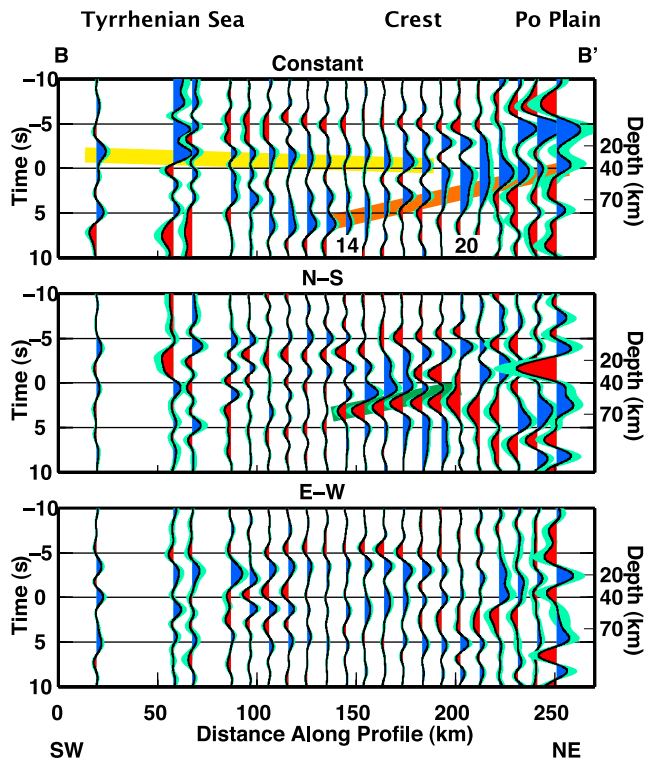


Figure 7. Similar to Figure 6, for profile  $BB'$ . In the upper panel the numbers below the traces indicate the spot numbers mentioned in text.

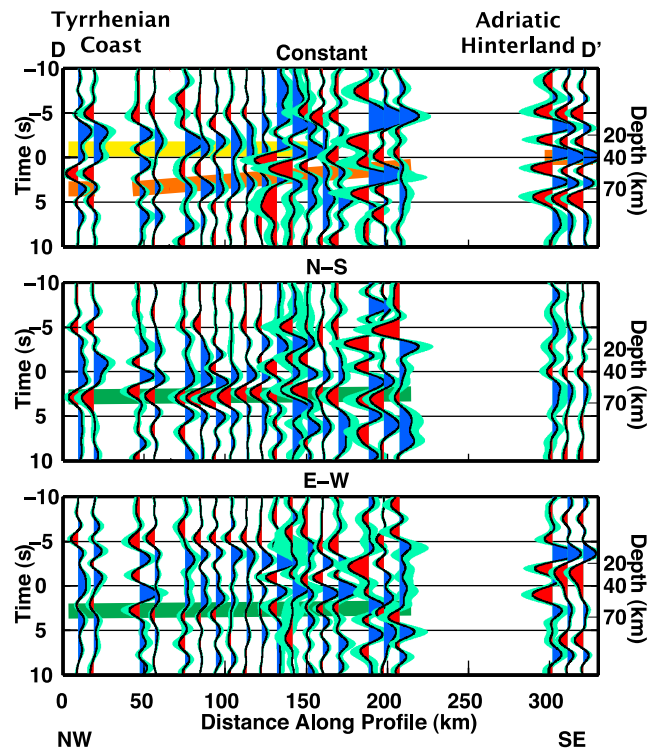


Figure 9. Similar to Figure 6, for profile  $DD'$ .

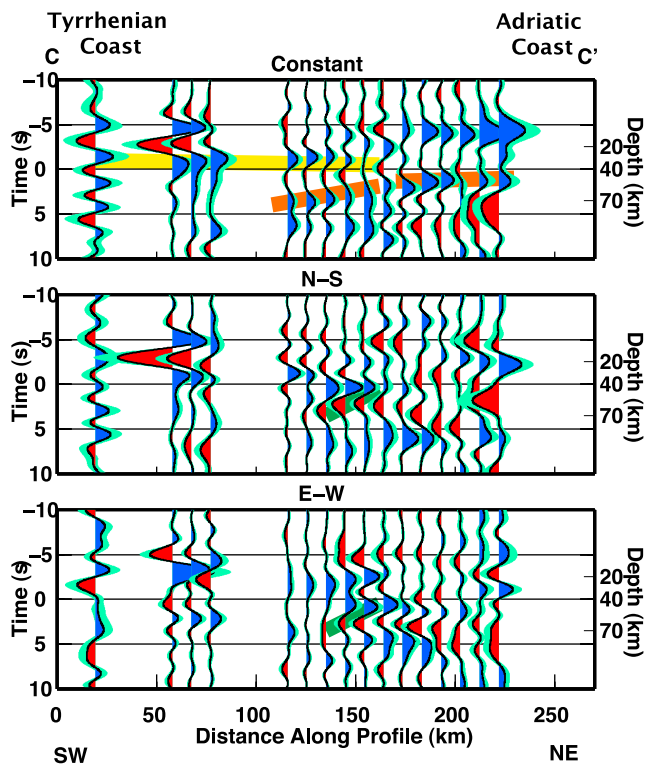


Figure 8. Similar to Figure 6, for profile  $CC'$ .

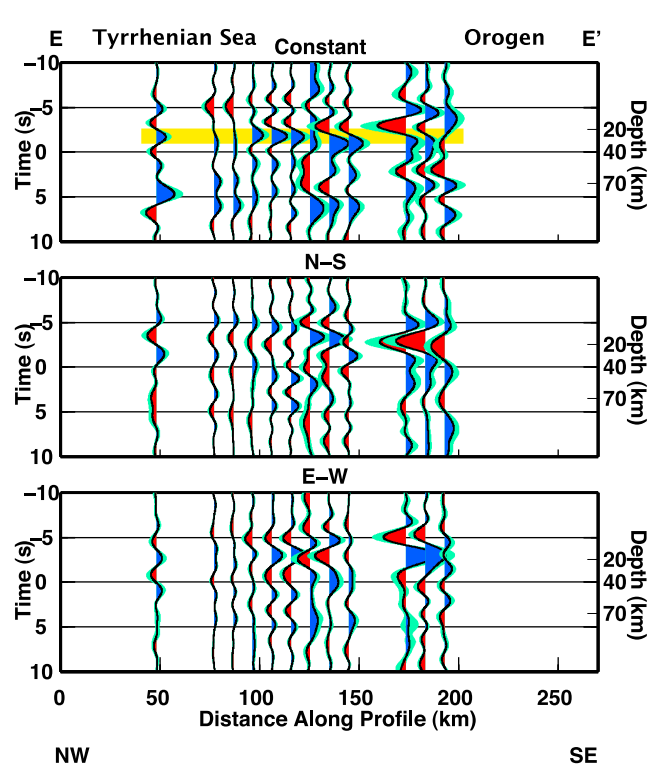
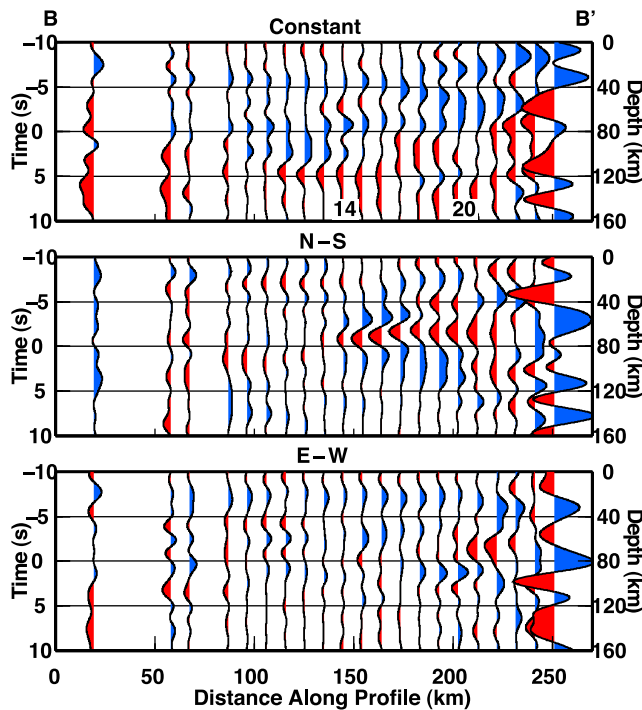


Figure 10. Similar to Figure 6, for profile  $EE'$ .



**Figure 11.** Similar to Figure 7, except that the RF are migrated to 80-km depth.

we infer a predominant NS-orientation of the structural features causing it.

[22] Profile  $AA'$  starts from the Ligurian Sea and ends at the (suggested) trench (Figure 6). It displays the same features described for profile  $BB'$ , with the exception that here the signal looks cleaner and less noisy. On the constant component a pulse is evident in the central part of the profile ( $X = 140 - 190$  km) at about  $-1.5$  s, and it becomes unclear toward the NE. A pulse, which displays an increasing delay time toward SW, appears in the NE side at  $1.5$  s, and it is present along the profile until the Tyrrhenian coast. Also, the  $\cos\phi$  back-azimuth harmonic displays features similar to profile  $BB'$ , i.e., the double dipping phase.

[23] Profile  $CC'$  runs parallel to profiles  $AA'$  and  $BB'$  but does not cross normal to the trench due to the local curvature of the chain (Figure 8). On the constant component we highlight a positive pulse shallowing from  $-0.5$  s on the Tyrrhenian coast line, to  $-1.5$  s at about  $X = 130$  km. On the Adriatic side, a positive pulse appears at progressively earlier times, from  $3.5$  s at  $100$  km along the profile to  $0.5$  s at roughly  $X = 140$  km. The time delay of this pulse flattens until  $X = 210$  km. On the profile  $CC'$  the segment where the two positive pulses overlap is shorter ( $<50$  km) than on  $BB'$ . Along this overlap, there is energy present in roughly equal measure on the  $\cos\phi$  and  $\sin\phi$  back-azimuth harmonics, suggesting a NE-SW orientation of features causing it.

[24] Profiles  $DD'$  and  $EE'$  parallel the orogen in its northern part, departing from it at the southern end (Figures 9 and 10). Owing to their geometry, we expect complex patterns in the pulses identified on the orogen-normal transects. For profile  $DD'$ , on the constant back-azimuth harmonic we observe two pulses throughout its length. The shallower one is located at about  $-1.5$  s on the Tyrrhenian side of the profile and maintains the same arrival time until  $X = 150$  km along profile,

where it disappears. The second one appears at about  $4$  s and is clear from  $X = 0$  to  $X = 120$  km; later it shallows to  $0$  s at the southeastern end of the profile. Near the Apennines crest the  $\cos\phi$  back-azimuth harmonic exhibits a double pulse at  $3.5$  s similar to those seen in profile  $BB'$ . There is also some energy in the  $\sin\phi$  back-azimuth harmonic at the same arrival time from  $X = 0$  to about  $X = 210$  km, displaying larger amplitude from  $X = 140$  to  $X = 210$  km. This likely indicates a variation in the symmetry directions from about N-S to NE-SW. Profile  $EE'$  runs along the Tyrrhenian side and ends near the Apennines orogen. We only observe a sharp pulse at  $-1$  s, and no energy appears in our targeted time window between  $0$  and  $4$  s on the  $\cos\phi$  and  $\sin\phi$  back-azimuth harmonics.

### 3.2. Summary of Observations

[25] The constant back-azimuth harmonic is influenced mainly by the isotropic seismic structure. Relative to our targeted  $Ps$  conversion depth of  $40$  km, we find a positive pulse in all profiles between  $-1.5$  and  $0.5$  s, mainly along the Tyrrhenian side but displaying variable expression toward the mountain chain. We associate this arrival with a positive velocity jump (i.e., a seismic discontinuity where velocity increases with depth) at relatively shallow depth. The Tyrrhenian Moho has been previously imaged as a shallow discontinuity in the work of *Piana Agostinetti et al.* [2008a]. Our results confirm this hypothesis. The low amplitude of this  $Ps$  conversion along all the profiles suggests the presence of a small impedance contrast between the crust and the upper mantle in this area. We observe another positive phase, recognizable along all profiles which run into the Adriatic domain, in the  $0-6$  s time window. This phase arrives progressively later from roughly east to west, dipping under the chain where it meets the earlier arrival from the Tyrrhenian Moho. We interpret this arrival as the  $P$ -to- $S$  converted phase from the Adriatic Moho. The Adriatic Moho has been detected at  $35-40$  km, and in some cases as deep as  $54$  km depth, across the Apennines, in a neighboring area [*Roselli et al.*, 2008]. In the Adriatic foredeep, the depth of this interface is debated [*Piana Agostinetti et al.*, 2002; *Levin et al.*, 2002a].

[26] Looking at the  $\cos\phi$  and  $\sin\phi$  plots gives us constraints on the 3D structure under this area. In general, the Tyrrhenian domain displays smaller amplitude in the  $k = 1$  harmonics  $\cos\phi$  and  $\sin\phi$  at our migration depth ( $40$  km). A strong double phase is seen along the entire chain where the two positive pulses overlap for the constant back-azimuth harmonic. This double phase seems to dip under the chain from the Adriatic toward the Tyrrhenian sea. While the above observations on the constant harmonic mainly confirm previous estimates of the crust-mantle boundary across the study area, the double-pulse directionally variable  $Ps$  phase, suggesting a layer trapped between two discontinuities, represents a new feature. We interpret this feature as defining a third structural zone along the Apennines, between the Tyrrhenian and the Adriatic, and here identified as the “overlapping” domain. Using this definition, we map the three areas in Figure 12. Moreover an additional analysis for profile  $BB'$  (Figure 11), where the focus of the migration is at  $80$  km depth, clearly shows that the double phase on the  $\cos\phi$  plot disappears at about  $80$  km depth (at  $X = 120$  km along profile  $BB'$ ).

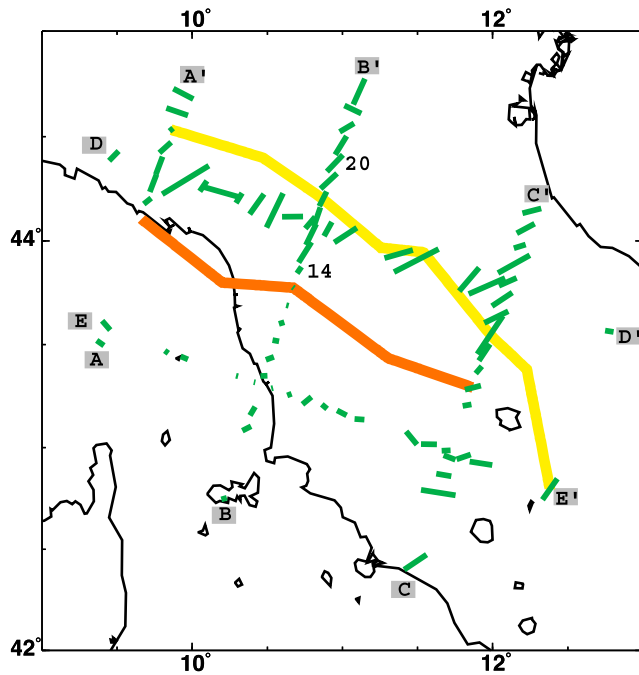


**Figure 12.** A map of symmetry directions (green sticks) obtained in the same way as the green arrow in Figure 5 for the time range 0–5 s in records migrated to 40-km depth. A yellow line shows the eastern boundary of the Tyrrhenian Moho; an orange line represents the western boundary of the Adriatic Moho, as identified in Figures 6–10.

[27] A double phase dipping toward the SW on the  $\cos\phi$  and  $\sin\phi$  plots could be explained by (1) a dipping isotropic layer bound by two interfaces with strong impedance contrasts or (2) a dipping anisotropic layer. In the first case, the observation of the double phases implies the presence of two strong impedance contrasts at the top and bottom interfaces. This model would also generate a dipping double phase on the constant back-azimuth harmonic, where we only find one positive pulse. On the other hand, the second case does not produce a double phase on the constant harmonic, if a weak seismic contrast is associated with the top interface. Thus we interpret the double phase in the  $\cos\phi$  and  $\sin\phi$  harmonics as an anisotropic layer which dips into the upper mantle toward the SW, roughly beneath the Apennines crest.

### 3.3. Symmetry Directions

[28] Following the approach described in the previous section, we obtain a symmetry direction for almost all the spots of each profile, corresponding to the major subcrustal  $P_s$  conversions at our target depth. In Figure 12, we plot all the directions found, together with the extension of the three zones defined above: Tyrrhenian, Overlapping, and Adriatic. The length of the arrow is proportional to the amplitudes of the pulses on the  $\cos\phi$  and  $\sin\phi$  plots. Well-defined patterns are present in the map, e.g., from the 14th to 20th spot along profile  $BB'$ , that allow us to draw interesting observations. First, we notice that in the Overlapping zone anisotropy axes have almost the same direction. In particular, in the portion of this zone where the horizontal distance between the two Mohos is larger, symmetry directions are consistent and display a NNE general trend. Where two Mohos are closer

(SE part of the area) symmetry directions are less uniform. Along the Tyrrhenian Sea the symmetry axes are relatively shorter than close to the mountains, suggesting weaker anisotropy. Their direction pattern is toward the southeast. On the Adriatic side, symmetry axes do not display a unique orientation. They twist toward the NW in the northern part and toward the NE and seldom SE in the southern part of the area, describing a fan-like pattern.

### 3.4. Modeling

[29] All observations drawn in the previous section need to be integrated in a model of the seismic structure across the study area, which can be discussed and compared to structures found in previous studies, or represented by geodynamic models. Thanks to the observations on the data set we are able to define three models, each corresponding to one of the illustrated zones (Figure 13). Computed synthetics (Figure 14) give a good representation of the observed RF traces. The main features shown by the cartoon in Figure 13 are (1) a flat shallow Moho on the Tyrrhenian side, (2) a dipping and deeper Moho on the Adriatic side, and (3) both isotropic features together, with an anisotropic layer above the deeper discontinuity, in the Overlapping area. Seismic wave speeds used to compute RF traces in Figure 14 are presented in Table 1. The anisotropic layer in the Overlapping zone is modeled using hexagonal anisotropy with a dipping symmetry axis. The axis trends  $N32^\circ E$ , being the average of the symmetry directions obtained along the transect (Figure 12), and plunges by  $20^\circ$  from the horizontal, indicative of the average value. The layer has 4% P and S wave speed anisotropy. In the Overlapping and Adriatic zones, the deepest interface is dipping  $20^\circ$  toward SSW, representing the dipping Moho of the Adriatic plate.

## 4. Discussion

[30] In this work, we implemented a new method to image the northern Apennines subduction zone. We investigated teleseismic receiver functions using a Common Conversion Point (CCP) procedure with the aim of creating 2D profiles of the subsurface structure. The recovered radial and transverse RFs are used to create three back-azimuth harmonics for each profile representing both isotropic and anisotropic structures. We divide the northern Apennines into three zones, Tyrrhenian, Adriatic, and Overlapping, on the basis of their seismic characterization, and to resolve the anisotropic features. We model the three zones with simple velocity structures to represent the main features highlighted in the RF gathers. The three models together delineate a realistic explanation of subsurface structures and produce a synthetic data-set similar to the observed (Figure 13).

[31] Our results for the Tyrrhenian side show a simple layer-over-half-space structure, where the main features of our data set confirm the presence of a flat horizontal discontinuity at  $\sim 25$  km depth, possibly associated with the Moho discontinuity. This Moho-like feature slightly deepens toward the foreland, which is the same trend highlighted by active seismic studies [e.g., *Franco et al.*, 1998; *Barchi et al.*, 1998]. Our simple modeling approach does not allow us to investigate the strength of the seismic velocity jump associated with this discontinuity, and our migrated sections do not demand strong anisotropy in the uppermost mantle beneath this shallow

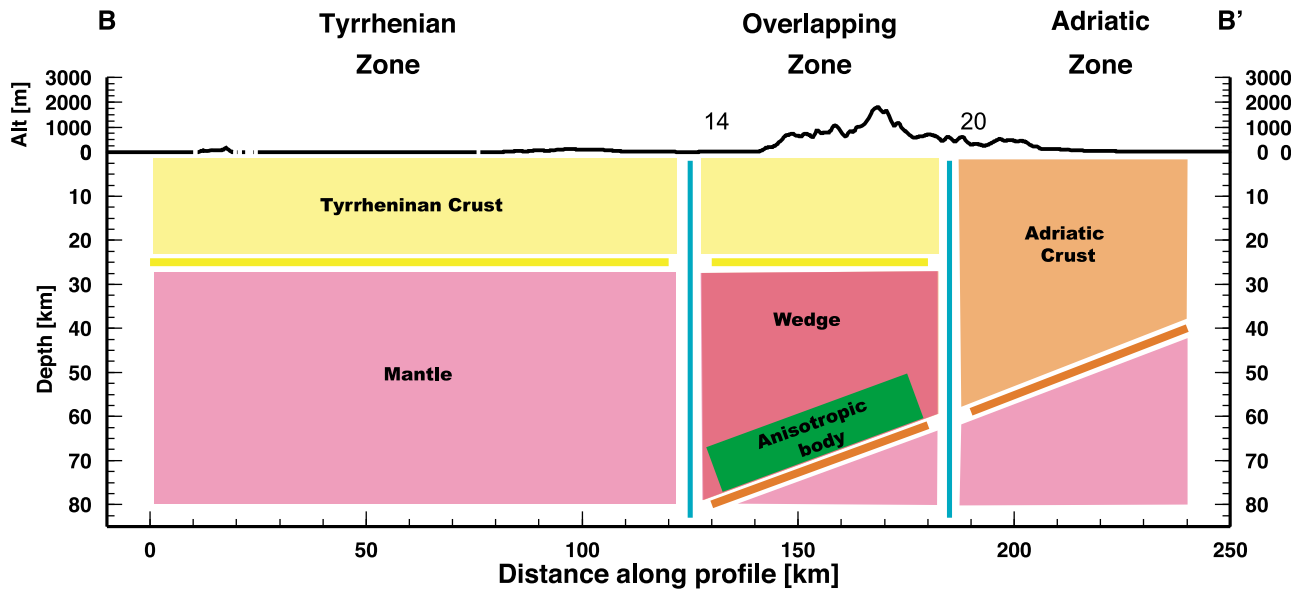


**Figure 13.** A 2-D schematic representation of the structures inferred along profile *BB'*. The profile is divided into three zones whose boundaries are represented by spots 14 and 20 in profile *BB'*.

interface. For the Adriatic side, the application of our method gives new insights into the subsurface seismic structure. A clear picture of the downgoing Adriatic Moho is retrieved. Classical RF analysis involving only the Q RF data set did not clearly image this discontinuity [Piana Agostinetti et al., 2008a]. Single station analysis suggests the presence of dip-

ping boundaries beneath the foreland of NA subduction [Piana Agostinetti and Amato, 2009]. Differing estimates for Moho depth along the Adriatic coast were reported by Piana Agostinetti et al. [2002] and Levin et al. [2002a]. The existence of thicker crust on the Adriatic side is consistent with the thermomechanical model of slab rollback developed by Pauselli and Federico [2002].

[32] Numerous studies performed along the CROP03 profile located at the southern end of the area investigated in this paper provide a similar picture of these two interfaces, in terms of their lateral extent, geometry, and the fact of their overlap [Barchi et al., 2006, and references therein]. The main finding of our analysis is the evidence for and the clear definition of the Overlapping domain where both Tyrrhenian and Adriatic Mohos are present. Moho doubling has been previously suggested in the study area [Ponziani et al., 1995] but only in a limited part of the NA chain.

[33] Our analysis allows us to characterize the Overlapping area in detail, including its lateral extent, and the separation between the two interfaces. Furthermore, our harmonic decomposition suggests the presence of an anisotropic body trapped between the two interfaces. The similarity of symmetry axes retrieved by our analysis implies coherence of

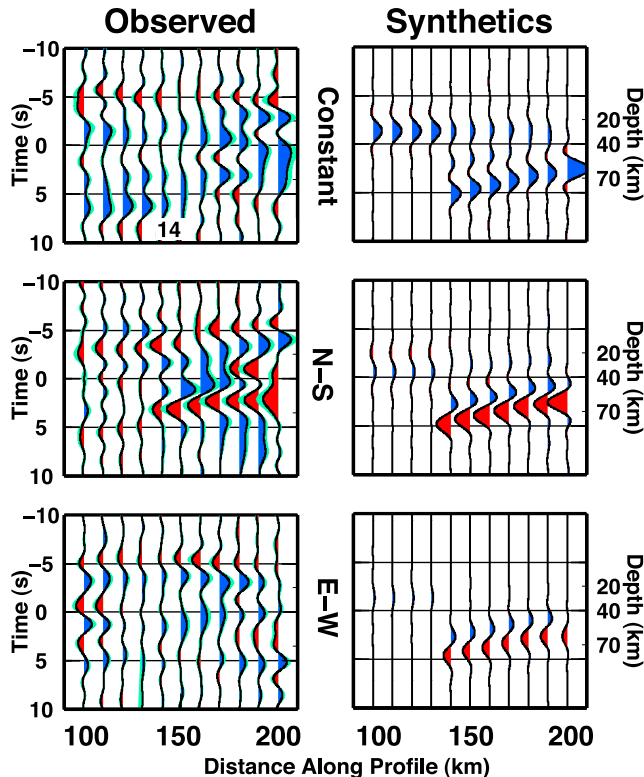


**Figure 14.** A subset of the profile *AA'* (Figure 6) compared with corresponding synthetic RFs computed from the models illustrated in Figure 13.

**Table 1.** Seismic Velocity for Models in Figure 14<sup>a</sup>

Type	Thick (km)	Vs
<i>Tyrrhenian</i>		
Crust	25	3.4
Mantle	Halfspace	4.1
<i>Overlapping</i>		
Crust	25	3.4
Wedge	38–21	3.8
Anisotropic layer	15	3.8
Mantle	Halfspace	4.2
<i>Adriatic</i>		
Crust	58–40	3.4
Mantle	halfspace	4.1

<sup>a</sup>Seismic velocity is measured in km/s.

anisotropic directions in the surrounding rock masses. The anisotropic body is characterized by significant anisotropy and regionally coherent orientation. In the Overlapping zone, the anisotropy directions show a coherent NNE trend (i.e., almost trench normal), rotating toward SW–NE further south in the orogen and suggesting a relationship between the anisotropic direction and the deformation field in the downgoing crust. On the other hand, in the NE side of the orogen, the anisotropic axes display a fan-like pattern probably indicating a SW-directed flow, while on the Tyrrhenian side anisotropy directions form a less coherent pattern, and imply low levels of anisotropy overall.

[34] The nature of the anisotropic body is not completely revealed from our simple analysis and modeling, but a comparison with other studies helps to identify promising hypotheses. Shear wave birefringence in the region [Plomerova *et al.*, 2006; Salimbeni *et al.*, 2007, 2008] shows a spatial pattern of anisotropic fast axes for SKS waves that displays an abrupt change across the Apennines, very similar to what we see in the distribution of anisotropic symmetry axes in the crust (Figure 12). However, the orientation of fast axes inferred from SKS splitting largely disagrees with those we infer, especially at the top of the subducting Apennines lithosphere. In the Adriatic domain SKS fast axes display some variation with event back azimuth, implying multilayered anisotropy [Salimbeni *et al.*, 2008, 2009].

[35] Because receiver functions and shear birefringence are sensitive to different spatial scales of the anisotropy, discrepancies in fast-axis orientation do not imply incompatible interpretations. Rather, they highlight the complexity of rock fabric beneath the northern Apennines and suggest the existence of at least two anisotropic features. The anisotropic signals we observe with receiver functions are generated by sharp contrasts in rock texture, typically within 5–20-km layers, and would lead to small ( $< 0.5$  s) birefringence time delays. Birefringence time delays of  $\delta t \simeq 1$  s likely accumulate through a substantial thickness of deformed rock, but if the anisotropic properties vary smoothly,  $P_s$  conversions are dampened and receiver-function signals would be weak or absent. In the Northern Apennines, the northward twist in fast-axis orientation on the convergent (Adriatic) side of the orogen from orogen-parallel to nearly orogen-normal has been attributed to either a preexisting mantle-lithosphere fabric [Plomerova *et al.*, 2006] or subslab asthenospheric flow associated with incipient slab detachment [Salimbeni *et al.*, 2007; Levin *et al.*, 2007]. The orientation of the birefringence fast-axis on the extensional (Tyrrhenian) side of the orogen trends NW to WNW, but this is where our cross-Apennines RF transect suggests that anisotropy is strongest, with symmetry axes roughly north–south.

[36] Disagreement between the anisotropic orientations inferred from shear wave birefringence and teleseismic receiver functions was reported in Tibet [Levin *et al.*, 2008], in Cascadia [Park *et al.*, 2004; Nikulin *et al.*, 2009], and in Kamchatka [Peyton *et al.*, 2001; Levin *et al.*, 2002b]. Better agreement with RF anisotropy is found for the birefringence of slab events in Kamchatka, which are insensitive to deeper deformation within and beneath the slab [Levin *et al.*, 2004].

[37] The degree of anisotropy in our models is greatest between 40 and 80 km depth, in a thin layer at the inferred top of the downgoing Apennines slab. The geometry suggests that this depth interval is where the slab first encounters

supraslab mantle, near the so-called mantle nose, where stresses in simple corner-flow models are infinite. We note that strong slabtop anisotropy has been inferred at depths to roughly 40 km in other subduction zone locales, particularly Cascadia [Nikulin *et al.*, 2009] and the Kii Peninsula, Japan [Shiomi and Park, 2008]. For both these locales  $P_s$  converted-wave amplitude appears weaker or absent for the slab interface at depths much greater than 40 km, in contrast to our observations from the Apennines slab. A difference in anisotropic character may indicate a distinct Apennines subduction dynamic or a distinct slab top lithology. The coincidence of high slab top anisotropy and nonvolcanic tremor in Cascadia and southern Japan suggests dehydration of hydrated rocks atop the oceanic crust, which in Cascadia may include the antigorite polymorph of serpentine [Nikulin *et al.*, 2009]. In the northern Apennines, our synthetic seismogram modeling can match the major features of the stacked receiver functions without the unusually low  $V_p$  and high  $V_p/V_s$  ratio of a serpentinite layer. Other geologic processes should be considered.

[38] It is simplest to associate anisotropy at the slab top with shear coupling between the slab and the overlying mantle, but a recent compilation of subduction zone studies argue against simple corner flow models [Long and Silver, 2008]. Katayama and Karato [2006] argue that many puzzling aspects of anisotropy in subduction zones can be related to factors that influence crystallographic transitions between modes of olivine deformation. Kneller *et al.* [2005] argued from geodynamics modeling that subduction zones should exhibit a partial decoupling from the mantle nose to the depth beneath the line of arc volcanoes. Abt *et al.* [2009] argue that such decoupling is necessary for the maintenance of along-trench flow consistent with trench-parallel birefringence fast axes in Costa Rica. Pinero-Feliciangelia and Kendall [2008] detect weak supraslab birefringence at many locations in the Caribbean, consistent with the partially decoupled hypothesis of Kneller *et al.* [2005]. Kawakatsu and Watada [2007] attribute a weakening in  $P_s$  converted-wave amplitude at roughly 50 km depth in Japan to slab dehydration and mineralogical transitions. Strong slabtop anisotropy in the northern Apennines persists to 80 km depth, which suggests that its expression of anisotropy differs from typical subduction zones.

[39] Geodetic observations for the northern Apennines [Serpelloni *et al.*, 2005] indicate that ongoing compression at the Po Valley thrust front is weak, and net convergence across the Apennines orogen is cancelled by extension in the “back-arc” region of Tuscany. Absent or weak convergence across a nominal subduction zone opens the possibility for a postsubduction delamination [e.g., Gogus and Pysklywec, 2008] to explain the synconvergent extension and uplift of central Italy. In this context the slab-top anisotropic layer that we detect could be associated with a boundary layer of highly deformed peridotite induced by the extreme stresses associated with lithospheric detachment. The well-documented existence of two Moho-like reflectors at the nominal point of detachment raises the possibility that this deformed layer was originally lower crust of the Adria microplate. More speculatively, such a layer could be the precursor of an ultra-high pressure (UHP) unit of metamorphosed crustal rocks or partially serpentinitized mantle rocks. First caught in the subduction channel, the layer would eventually rise buoyantly toward the surface.

[40] Geodynamic models for UHP exhumation typically predict the detachment and subduction of low-density rocks to form a deformed layer atop the downgoing slab during a continental collision [Warren *et al.*, 2008a, 2008b]. Within our field area, the Alpi Apuane marbles were subjected to lower-crustal metamorphism (15–30 km at 20 Ma) and have been exhumed from 9 km depth since 10–13 Ma [Fellin *et al.*, 2007]. More broadly, apatite thermochronology [Thomson *et al.*, 2010] constrains uplift to have occurred across the entire Northern Apennines orogen during the past few Myr, with a pattern of exhumation that suggests slab delamination, rather than subduction convergence, in the region sampled by our transects  $B - B'$  and  $A - A'$ . No UHP terranes have been reported in the Northern Apennines, but the orogen is relatively young. UHP terranes exposed by deeper exhumation are found nearby in the Alps [Skemer *et al.*, 2006; Federico *et al.*, 2007; Jung, 2009], an older zone of continental collision. Further study of deep anisotropic features in the Apennines orogen will be necessary to determine if it indeed harbors a future exhumed UHP terrane.

## 5. Conclusion

[41] In this paper, we present a new methodology for the analysis of RF data sets and apply it to a large teleseismic data set collected across the northern Apennines orogen (Italy). The method successfully exploits the information contained in both radial and transverse receiver functions giving better constraints on the subsurface seismic structure than radial-only receiver function analysis. A harmonic decomposition is used to retrieve the isotropic structure under the seismic stations and to focus on buried anisotropic bodies. Using a CCP approach, we are able to image the lateral continuity of such anisotropic bodies at depth and to map the anisotropic axis directions across the whole study area.

[42] The application of this new technique to the RETREAT data set improves the knowledge of the uppermost mantle structure in the Northern Apennines area. The new analysis of the RF data set defines an area along the Apennines chain where the Adriatic and Tyrrhenian Moho discontinuities appear to overlap. An anisotropic body is found trapped between these two discontinuities. The anisotropic axis of this body is oriented trench-normal, including a rotation of the axis from NNE to NE as the Apennines strike turns toward the south. The layer could be subducted crust, but the depth extent of its apparent anisotropy is greater than for subduction zones in Japan and Cascadia, suggesting that hydrated oceanic crust is not present. We hypothesize that the anisotropic body is the remnant of the delamination of the Adriatic microplate lower crust, continental in character. A sheared layer of mantle wedge peridotite atop the Apennines slab is an alternate hypothesis, but the RFs do not require low  $V_p$  and high  $V_p/V_s$  ratios, that is, the characteristics of strong serpentinization. Rather, geologic evidence for prolonged recent uplift in the Northern Apennines favors the hypothesis that subducted lower crust may be rising buoyantly from depth as a future UHP terrane.

[43] **Acknowledgments.** The RETREAT field campaign was funded by NSF Continental Dynamics, and received significant support from INGV and the Geophysical Institute, Prague. Data collection was facilitated in part by IRIS PASSCAL, data archival provided by the IRIS DMC. IB is

supported by DPC-S1\_UR02.02 and by the CNT section of INGV, Rome. NPA was supported by project Airplane (funded by the Italian Ministry of Research, project RBPR05B2ZJ\_003). JP and VL were supported by NSF grant EAR-0208652. IB thanks Mark Brandon for financial support, Francesco Pio Lucente for helpful discussions, and Pamela Roselli for the selection of the data set at ARZ station. GMT [Wessel and Smith, 1991] was used for developing figures.

## References

- Abt, D. L., K. M. Fischer, G. A. Abers, W. Strauch, J. M. Protti, and V. Gonzalez (2009), Shear wave anisotropy beneath Nicaragua and Costa Rica: Implications for flow in the mantle wedge, *Geochem. Geophys. Geosyst.*, *10*, Q05S15, doi:10.1029/2009GC002375.
- Bannister, S., M. Reyners, G. Stuart, and M. Savage (2007), Imaging the Hikurangi subduction zone, New Zealand, using teleseismic receiver functions: Crustal fluids above the forearc mantle wedge, *Geophys. J. Int.*, *169*(2), 602–616.
- Barchi, M. R., G. Minelli, and G. Piali (1998), The crop 03 profile: A synthesis of results on deep structures of the Northern Apennines, *Mem. Soc. Geol. It.*, *52*, 383–400.
- Barchi, M. R., C. Pauselli, C. Chiarabba, R. Di Stefano, C. Federico, and G. Minelli (2006), Crustal structure, tectonic evolution and seismogenesis in the Northern Apennines (Italy), *Boll. Geof. Teor. Appl.*, *0006–6729*(47), 249–270.
- Bianchi, I., N. Piana Agostinetti, C. Chiarabba, and P. De Gori (2008), Deep structure of the Colli Albani volcanic district (central Italy) from receiver functions analysis, *J. Geophys. Res.*, *113*, B09313, doi:10.1029/2007JB005548.
- Channell, J. E. T., and J. C. Mareschal (1989), Delamination and asymmetric lithospheric thickening in the development of the Tyrrhenian Rift, *Geol. Soc. London Spec. Publ.*, *45*, 285–302.
- Chiarabba, C., L. Jovane, and R. D. Stefano (2005), A new view of Italian seismicity using 20 years of instrumental recordings, *Tectonophysics*, *395*, 251–268.
- De Luca, G., M. Cattaneo, G. Monachesi, and A. Amato (2009), Seismicity in central and northern Apennines integrating the Italian national and regional networks, *Tectonophysics*, *476*, 121–135, doi:10.1016/j.tecto.2008.11.032.
- Di Stefano, R., E. Kissling, C. Chiarabba, A. Amato, and D. Giardini (2009), Shallow subduction beneath Italy: Three-dimensional images of the Adriatic-European-Tyrrhenian lithosphere system based on high-quality P wave arrival times, *J. Geophys. Res.*, *114*, B05305, doi:10.1029/2008JB005641.
- Dueker, K. G., and A. F. Sheehan (1998), Mantle discontinuity structure beneath the Colorado Rocky Mountains and High Plains, *J. Geophys. Res.*, *103*(B4), 7153–7169.
- Faccenna, C., T. W. Becker, F. P. Lucente, L. Jolivet, and F. Rossetti (2001), History of subduction and back-arc extension in the Central Mediterranean, *Geophys. J. Int.*, *145*, 809–820.
- Faccenna, C., C. Piromallo, A. Crespo-Blanc, L. Jolivet, and F. Rossetti (2004), Lateral slab deformation and the origin of the Western Mediterranean arc, *Tectonics*, *23*, TC1012, doi:10.1029/2002TC001488.
- Federico, L., L. Crispini, M. Scambelluri, and G. Capponi (2007), Ophiolite melange zone records exhumation in a fossil subduction channel, *Geology*, *35*, 499–502, doi:10.1130/G23190A.1.
- Fellin, M. G., P. W. Reiners, M. T. Brandon, E. Wuthrich, M. L. Balestrieri, and G. Molli (2007), Thermochronologic evidence for the exhumational history of the Alpi Apuane metamorphic core complex, Northern Apennines, Italy, *Tectonics*, *26*, TC6015, doi:10.1029/2006TC002085.
- Ferris, A., G. A. Abers, D. H. Christensen, and E. Veenstra (2003), High resolution image of the subducted Pacific (?) plate beneath central Alaska, *Earth Planet. Sci. Lett.*, *214*(3–4), 575–588.
- Franco, R. D., F. Ponziani, G. Biella, G. Boniolo, G. Caielli, A. Corsi, M. Maistrello, and A. Morrone (1998), DSS-WAR experiment in support of the CROP-03 project, *Mem. Soc. Geol. It.*, *52*, 67–90.
- Frederiksen, A. W., and M. G. Bostock (2000), Modeling teleseismic waves in dipping anisotropic structures, *Geophys. J. Int.*, *141*, 401–412.
- Girardin, N., and V. Farra (1998), Azimuthal anisotropy in the upper mantle from observation of P-to-S converted phases: Application to southeast Australia, *Geophys. J. Int.*, *133*, 615–629.
- Gogos, O. H., and R. N. Pysklywec (2008), Mantle lithosphere delamination driving plateau uplift and synconvergent extension in eastern Anatolia, *Geology*, *36*, 723–726.
- Jung, H. (2009), Deformation fabrics of olivine in Val Malenco peridotite found in Italy and implications for the seismic anisotropy in the upper mantle, *Lithos*, *109*, 341–349.
- Katayama, I., and S.-I. Karato (2006), Effect of temperature on the B- to C-type olivine fabric transition and implication for flow pattern in subduction zones, *Phys. Earth Planet. Int.*, *157*, 33–45.

- Kawakatsu, H., and S. Watada (2007), Seismic evidence for deep-water transportation in the mantle, *Science*, *306*, 1468–1471.
- Keogh, P., J. Adam, and P. Lebedev (2009), A surface-wave study of structure and anisotropy of Tuscany, *Eos Trans. AGU*, *90*(52), Fall Meet. Suppl., Abstract T51B-1524.
- Kneller, E. A., P. E. van Keken, S.-I. Karato, and J. Park (2005), B-type fabric in the mantle wedge: Insights from high-resolution non-Newtonian subduction zone models, *Earth Planet. Sci. Lett.*, *237*, 781–797.
- Langston, C. A. (1979), Structure under Mount Rainier, Washington, inferred from teleseismic body waves, *J. Geophys. Res.*, *84*(B9), 4749–4762.
- Levin, V., and J. Park (1997), P-SH conversions in a flat-layered medium with anisotropy of arbitrary orientation, *Geophys. J. Int.*, *131*(2), 253–266.
- Levin, V., and J. Park (1998), P-SH conversions in layered media with hexagonally symmetric anisotropy: A cookbook, *Pure Appl. Geophys.*, *151*(2–4), 669–697.
- Levin, V., L. Margheriti, J. Park, and A. Amato (2002a), Anisotropic seismic structure of the lithosphere beneath the Adriatic coast of Italy constrained with mode-converted body waves, *Geophys. Res. Lett.*, *29*(22), 2058, doi:10.1029/2002GL015438.
- Levin, V., J. Park, M. Brandon, J. Lees, V. Peyton, E. Gordeev, and A. Ozerov (2002b), Crust and upper mantle of Kamchatka from teleseismic receiver functions, *Tectonophysics*, *358*, 233–265.
- Levin, V., D. Droznin, J. Park, and E. Gordeev (2004), Mantle wedge anisotropy beneath southeastern Kamchatka from local-S birefringence, *Geophys. J. Int.*, *158*, 1009–1023.
- Levin, V., J. Park, F. P. Lucente, L. Margheriti, and S. Pondrelli (2007), End of subduction in Northern Apennines confirmed by observations of quasi-Love waves from the great 2004 Sumatra-Andaman earthquake, *Geophys. Res. Lett.*, *34*, L04304, doi:10.1029/2006GL028860.
- Levin, V., S. Roecker, P. Graham, and A. Hosseini (2008), Seismic anisotropy indicators in Western Tibet: Shear wave splitting and receiver function analysis, *Tectonophysics*, *462*, 99–108.
- Li, H., F. Bernardi, and A. Michelini (2010), Surface wave dispersion measurements from ambient seismic noise analysis in Italy, *Geophys. J. Int.*, *180*(3), 1242–1252.
- Long, M. D., and P. G. Silver (2008), The subduction zone flow field from seismic anisotropy: A global view, *Science*, *319*, 315–318.
- Lucente, F. P., C. Chiarabba, G. B. Cimini, and D. Giardini (1999), Tomographic constraints on the geodynamic evolution of the Italian region, *J. Geophys. Res.*, *104*, 20,307–20,327.
- Malinverno, A., and W. B. F. Ryan (1986), Extension in the Tyrrhenian sea and shortening in the Apennines as results of arc migration driven by sinking of the lithosphere, *Tectonics*, *5*, 227–245.
- Margheriti, L., et al. (2006), RETREAT seismic deployment in the northern Apennines, *Ann. Geofis.*, *49*(4/5), 1119–1131.
- Maupin, V., and J. Park (2007), Theory and observations: Wave propagation in anisotropic media, in *Treatise on Geophysics, Seismology and Structure of the Earth*, vol. 1, edited by B. Romanowicz and A. Dziewonski, pp. 289–321, Elsevier, New York.
- Mercier, J.-P., M. G. Bostock, P. Audet, J. B. Gaherty, E. J. Garnero, and J. Revenaugh (2008), The teleseismic signature of fossil subduction: Northwestern Canada, *J. Geophys. Res.*, *113*, B04308, doi:10.1029/2007JB005127.
- Nikulin, A., V. Levin, and J. Park (2009), Receiver function study of the Cascadia megathrust: Evidence for localized serpentinization, *Geochem. Geophys. Geosyst.*, *10*, Q07004, doi:10.1029/2009GC002376.
- Park, J., and V. Levin (2000), Receiver functions from multiple-taper spectral correlation estimates, *Bull. Seismol. Soc. Am.*, *90*, 1507–1520.
- Park, J., H. Yuan, and V. Levin (2004), Subduction zone anisotropy beneath Corvallis, Oregon: A serpentinite skid mark of trench-parallel terrane migration?, *J. Geophys. Res.*, *109*, B10306, doi:10.1029/2003JB002718.
- Pauselli, C., and C. Federico (2002), The brittle/ductile transition along the crop03 seismic profile: Relationship with the geological feature, *Boll. Soc. Geol. It., Spec. 1*, 25–35.
- Pauselli, C., M.-R. Barchi, C. Federico, M. B. Magnani, and G. Minelli (2006), The crustal structure of the Northern Apennines (central Italy): an insight by the CROP03 seismic line, *Am. J. Sci.*, *306*, 428–450.
- Peacock, S. M., and K. Wang (1999), Seismic consequences of warm versus cool subduction metamorphism: Examples from southwest and northeast Japan, *Science*, *286*(5441), 937–939.
- Peyton, V., V. Levin, J. Park, M. T. Brandon, J. Lees, E. Gordeev, and A. Ozerov (2001), Mantle flow at a slab edge: Seismic anisotropy in the Kamchatka region, *Geophys. Res. Lett.*, *28*, 379–382.
- Piaili, G., M. Barchi, and G. Minelli (1998), Results of the CROP 03 deep seismic reflection profile, *Mem. Soc. Geol. It.*, *52*, 647.
- Piana Agostinetti, N., and A. Amato (2009), Moho depth and  $v_p/v_s$  ratio in peninsular Italy from teleseismic receiver functions, *J. Geophys. Res.*, *114*, B06303, doi:10.1029/2008JB005899.
- Piana Agostinetti, N., F. P. Lucente, G. Selvaggi, and M. Di Bona (2002), Crustal structure and Moho geometry beneath the Northern Apennines (Italy), *Geophys. Res. Lett.*, *29*(20), 1999, doi:10.1029/2002GL015109.
- Piana Agostinetti, N., V. Levin, and J. Park (2008a), Crustal structure above a retreating trench: Receiver function study of the Northern Apennines orogen, *Earth Planet. Sci. Lett.*, *275*(3–4), 211–220, doi:10.1016/j.epsl.2008.06.022.
- Piana Agostinetti, N., J. Park, and F. P. Lucente (2008b), Mantle wedge anisotropy in Southern Tyrrhenian subduction zone (Italy), from receiver function analysis, *Tectonophysics*, *462*(1–4), 35–48, doi:10.1016/j.tecto.2008.03.020.
- Piana Agostinetti, N., M. Steckler, and F. P. Lucente (2009), Imaging the subducted slab under the Calabrian Arc, Italy, from receiver function analysis, *Lithosphere*, *1*(3), 131–138, doi:10.1130/L49.1.
- Piccinini, D., C. Chiarabba, A. Aguilera, and Monghidoro Earthquake Group (2006), Compression along the Northern Apennines? Evidence from the Mw 5.3 Monghidoro earthquake, *Terra Nova*, *18*, 89–94, doi:10.1111/j.1365-3121.2005.00667.
- Piccinini, D., N. Piana Agostinetti, P. Roselli, M. Ibs-von Seht, and T. Braun (2009), Analysis of small magnitude seismic sequences along the Northern Apennines (Italy), *Tectonophysics*, *476*, 136–144, doi:10.1016/j.tecto.2009.04.005.
- Picotti, V., and F. J. Pazzaglia (2008), A new active tectonic model for the construction of the Northern Apennines mountain front near Bologna (Italy), *J. Geophys. Res.*, *113*, B08412, doi:10.1029/2007JB005307.
- Pinero-Feliciangelia, L. T., and J.-M. Kendall (2008), Sub-slab mantle flow parallel to the Caribbean plate boundaries: Inferences from SKS splitting, *Tectonophysics*, *462*, 22–34, doi:10.1016/j.tecto.2008.01.022.
- Plomerova, J., et al. (2006), Seismic anisotropy beneath the Northern Apennines (Italy): Mantle flow or lithosphere fabric?, *Earth Planet. Sci. Lett.*, *247*, 157–170.
- Ponziani, F., R. D. Franco, G. Minelli, G. Biella, C. Federico, and G. Piaili (1995), Crustal shortening and duplication of the Moho in the Northern Apennines: A view from seismic refraction data, *Tectonophysics*, *252*, 391–418.
- Roselli, P., F. P. Lucente, and N. Piana Agostinetti (2008), Crustal structure at colliding plates boundary from receiver functions analysis: A close look beneath the Northern Apennines (Italy), *Geophys. Res. Lett.*, *35*, L12304, doi:10.1029/2008GL034055.
- Roselli, P., N. Piana Agostinetti, and T. Braun (2010), Shear-velocity and anisotropy structure of a retreating extensional forearc (Tuscany, Italy) from receiver functions inversion, *Geophys. J. Int.*, *181*, 545–556, doi:10.1111/j.1365-246X.2010.04520.x.
- Salimbeni, S., S. Pondrelli, L. Margheriti, V. Levin, J. Park, J. Plomerova, and V. Babuska (2007), Abrupt change in mantle fabric across Northern Apennines detected using seismic anisotropy, *Geophys. Res. Lett.*, *34*, L07308, doi:10.1029/2007GL029302.
- Salimbeni, S., S. Pondrelli, L. Margheriti, J. Park, and V. Levin (2008), SKS splitting measurements beneath the Northern Apennines region: A case of oblique trench retreat, *Tectonophysics*, *462*(1–4), 68–82.
- Salimbeni, S., V. Levin, S. Pondrelli, L. Margheriti, and J. Park (2009), Distribution of seismic anisotropy beneath central Italy and geodynamic implications for Northern Apennines, *Eos Trans. AGU*, *90*(52), Fall Meet. Suppl., Abstract D113A-1673.
- Savage, M. (1998), Lower crustal anisotropy or dipping boundaries? Effects on receiver functions and a case of study in New Zealand, *J. Geophys. Res.*, *103*(15), 69–87.
- Serpelloni, E., M. Anzidei, P. Baldi, G. Casula, and A. Galvani (2005), Crustal velocity and strain-rate fields in Italy and surrounding regions: new results from the analysis of permanent and non-permanent GPS networks, *Geophys. J. Int.*, *161*(3), 861–880.
- Shiomi, K., and J. Park (2008), Structural features of the subducting slab beneath the Kii Peninsula, central Japan: Seismic evidence of slab segmentation, dehydration, and anisotropy, *J. Geophys. Res.*, *113*, B10318, doi:10.1029/2007JB005535.
- Skemer, P., I. Katayama, and S.-I. Karato (2006), Deformation fabrics of the Cima di Gagnone peridotite massif, Central Alps, Switzerland: Evidence of deformation at low temperatures in the presence of water, *Contrib. Mineral. Petrol.*, *152*, 43–51, doi:10.1007/s00410-006-0093-4.
- Thomson, S. N., M. T. Brandon, P. W. Reiners, M. Zattin, P. J. Isaacson, and M. L. Balestrieri (2010), Thermochronologic evidence for orogen-parallel variability in wedge kinematics during extending convergent orogenesis of the Northern Apennines, Italy, *Geol. Soc. Am. Bull.*, *122*(7/8), 1160–1179.
- Tibi, R., D. A. Wiens, and X. Yuan (2008), Seismic evidence for wide-spread serpentinized forearc mantle along the Mariana convergence margin, *Geophys. Res. Lett.*, *35*, L13303, doi:10.1029/2008GL034163.
- Tonegawa, T., K. Hirahara, T. Shibutani, H. Iwamori, H. Kanamori, and K. Shiomi (2008), Water flow to the mantle transition zone inferred from

- a receiver function image of the Pacific slab, *Earth Planet. Sci. Lett.*, *274*, 346–354, doi:10.1016/j.epsl.2008.07.046.
- Vinnik, L. P. (1977), Detection of waves converted from P to SV in the mantle, *Earth Planet. Inter.*, *15*, 39–45.
- Vinnik, L. P., I. M. Aleshin, S. G. Kiselev, G. L. Kosarev, and L. I. Makeyeva (2007), Depth localized azimuthal anisotropy from SKS and P receiver functions; the Tien Shan, *Geophys. J. Int.*, *169*(3), 1289–1299.
- Warren, C. J., C. Beaumont, and R. A. Jamieson (2008a), Formation and exhumation of ultra-high-pressure rocks during continental collision: Role of detachment in the subduction channel, *Geochem. Geophys. Geosyst.*, *9*, Q04019, doi:10.1029/2007GC001839.
- Warren, C. J., C. Beaumont, and R. A. Jamieson (2008b), Modelling tectonic styles and ultra-high pressure (UHP) rock exhumation during the transition from oceanic subduction to continental collision, *Earth Planet. Sci. Lett.*, *267*, 129–145.
- Wessel, P., and W. H. F. Smith (1991), Free software helps map and display data, *Eos Trans. AGU*, *72*, 441.
- Wilson, C. K., C. H. Jones, P. Molnar, A. F. Sheehan, and O. S. Boyd (2004), Distributed deformation in the lower crust and upper mantle beneath a continental strike-slip fault zone: Marlborough fault system, South Island, New Zealand, *Geology*, *32*, 837–84, doi:10.1130/G20657.1.
- Wilson, C. K., F. J. Pazzaglia, and D. J. Anastasio (2009), A fluvial record of active fault-propagation folding, Salsomaggiore anticline, Northern Apennines, Italy, *J. Geophys. Res.*, *114*, B08403, doi:10.1029/2008JB005984.
- 
- I. Bianchi and N. Piana Agostinetti, Centro Nazionale Terremoti, Istituto Nazionale di Geofisica e Vulcanologia, Via Vigna Murata 605, I-00143 Rome, Italy. (irene.bianchi@ingv.it)
- V. Levin, Department of Geological Sciences, Rutgers University, Wright Geological Laboratory, 610 Taylor Rd., Piscataway, NJ 08854, USA.
- J. Park, Department of Geology and Geophysics, Yale University, New Haven, CT 06511, USA.